Ab initio strategy for muon site assignment in wide band gap fluorides

F. Bernardini,[1] P. Bonfà,[2] S. Massidda,[1] and R. De Renzi[2]

[1]*CNR-IOM-Cagliari and Dipartimento di Fisica, Università di Cagliari, IT-09042 Monserrato, Italy*

[2]*Dipartimento di Fisica e Scienze della Terra and Unità CNISM di Parma, Università di Parma, I-43124 Parma, Italy*

(Received 16 January 2013; published 29 March 2013)

We report on an *ab initio* strategy based on density functional theory to identify the muon sites. Two issues must be carefully addressed: muon delocalization about candidate interstitial sites and local structural relaxation of the atomic positions due to μ^+-sample interaction. Here, we verify our strategy's validity focusing on two wide band gap materials, LiF and YF_3, where both μ^+ delocalization and crystal lattice relaxation play an important role in determining the μ^+ stopping site positions.

DOI: 10.1103/PhysRevB.87.115148 PACS number(s): 76.75.+i, 71.15.Mb, 76.60.Jx

I. INTRODUCTION

When collected into a high-intensity spin-polarized beam, muons become a powerful probe for many fields of physics and other scientific areas.[1–5] Many appealing characteristics have determined the success of muon spin rotation and relaxation spectroscopy (μSR). First, μSR significantly widens the set of materials that can be studied if compared to other spectroscopic techniques (e.g., NMR and ESR) since it can be applied to virtually any specimen by simply implanting muons. Secondly, during its lifetime the muon spin interacts with magnetic ordering of either nuclear or electronic origin, and provides information on local magnetic fields on a small length scale and—when fluctuating regimes are involved—on a large frequency window.[1,6] Thus, muons are mainly used as a microscopic magnetometer to probe both static and dynamic magnetic ordering. Relevant results have also been obtained when modeling the effects of hydrogenlike impurities in semiconductors, and their reaction kinetics, in order to study quantum diffusion.[7–9] Moreover, in spatially inhomogeneous systems, μSR gives valuable complementary results with respects to neutron diffraction and NMR since implanted muons probe the sample from the interstitial region far from nuclei. Nonetheless, the muon site assignment remains a long-standing problem and may represent a serious issue in many μSR experiments when it comes to extracting quantitative information from μSR data. After implantation, the positive muons (μ^+) usually stop at high-symmetry interstitial sites of the crystal lattice. In metals, a cloud of conduction electrons efficiently screens positive charges, so that muons leave the positions of neighboring atoms nearly unperturbed.[10] Instead, in insulators and semiconductors the final μ^+ sites can be in an off-center interstitial position because of the formation of chemical bonding between the muon and its neighboring atoms.[10–14] From the very beginning of μSR a lot of work has been devoted to the determination of the muon sites. In several materials a precise determination of muon interstitial sites was indeed possible thanks to accurate experimental studies of the Knight shift, of the level crossing resonance (LCR), and by inspecting asymmetry relaxation rates as a function of applied fields in selected compounds.[15–19] Nonetheless, there is also a large number of cases in which both muon position and muons' effect on the hosting system cannot be inferred solely by experimental knowledge; therefore, a reliable method to obtain muon sites in condensed matter would be of great value. To this aim, a variety of theoretical and computational approaches were used.[14,20–27] Successful results have been recently obtained for metallic compounds where an estimation based on the electrostatic potential enabled the identification of muon sites.[28]

In this work, we want to show that, among the many possible approaches[23,24,28,29] based on a first-principles method, density functional theory (DFT), already well known for its success in studying the electronic structure of solids, is also a powerful, accurate, and effective tool to explore the μ^+-sample interactions on a selected set of experimental acquisitions. Our work highlights that in insulators the use of a DFT approach is preferable since the stronger interaction with the local environment makes muon position identification a nonstraightforward task.

Here we present our results for two fluorine compounds, namely LiF and YF_3. They are very useful test cases for our computational investigation. Both materials' ground-state electronic structure is well reproduced by DFT. Therefore, we expect it to provide an accurate value for the electrostatic potential and the local atomic structure surrounding the μ^+. Among the insulators, LiF and YF_3 are two well-studied cases in which a strong μ^+-lattice interaction develops. This leads to the formation of a trimer structure with an ionized μ^+ between two F nuclei, known as the F-μ^+-F complex.[11] The dipolar interaction between F and μ spins in F-μ^+-F produces a signature in the μSR signal. This allows an accurate determination of the μ^+-F distance, which we use to validate our calculations' results.[13]

The paper is organized as follows. In Sec. II we present the computational strategy for the identification of μ^+ sites, and in Sec. III we describe the procedure based on the solution of the Hamiltonian for the μ^+-F nuclear spin interactions allowing the determination of the local atomic environment from μSR spectra. In Secs. IV and V we discuss the outcome of our calculations on LiF and YF_3, respectively. Finally, we present a summary and the conclusions of our work in Sec. VI.

II. COMPUTATIONAL DETAILS

We use the generalized gradient approximation (GGA)[30] to the DFT and the pseudopotential-based plane-wave method (PPPW) as implemented in the QUANTUM ESPRESSO (QE) package.[31] Li, Y, and F are slightly difficult elements for various reasons. F is a first-row element with a deep potential,

whereas Li and Y have shallow *s* semicore levels. To guarantee convergence, we used the projector augmented wave approach[32] with explicit treatment of the *s* semicore as valence and a plane-wave basis set up to 800 eV. The Brillouin zone integration is not a critical issue with wide band gap insulators, therefore a $8 \times 8 \times 8$ Monkhorst-Pack mesh for the bulk and $4 \times 4 \times 4$ for the supercell with a Gaussian smearing guarantees convergence. Since we are interested in the electrostatic potential generated by the electrons and nuclei, our calculations may be affected by the pseudoization of the potential inside the atomic core region. For this reason, we double-checked our muon distribution calculations by comparing the results we got for the perfect bulk system with full-potential calculations using the augmented plane wave plus local orbitals (APW + lo)[33,34] method as implemented in the WIEN2K package.[35] We found that muon positions are not affected by the electrostatic potential's approximate description due to the pseudoization.

The muon stopping site search problem can be approached as the solution for the motion of a particle slowing down in an effective potential given by a mean-field approximation. Here, in agreement with previous approaches,[28,36] we consider that the potential felt by the muon V_μ is the sum of the Hartree and nuclei terms:

$$V_\mu(\mathbf{r}) = -\frac{e^2}{2}\int \frac{n(\mathbf{r}')}{\mathbf{r}-\mathbf{r}'}dr' + \sum_i \frac{Z_i e^2}{\mathbf{r}-\mathbf{R}_i}. \quad (1)$$

We call this *the electrostatic approximation* and we disregard possible electron-muon correlation effects. V_μ has minima V_0 in the interstitial positions. Since muons are light-mass particles, the identification of the minima with stopping sites is not trivial. Indeed zero-point motion (ZPM) effects may play an important role in muon localization. LiF and YF_3 are good examples in this respect. Because of the ZPM, not all minima are stopping sites. If we have more than one minimum inside a primitive cell, the muon hops between neighboring sites if the barrier to be overtaken is lower than the ZPM energy. At the end the muon will stop in a minimum surrounded by barriers whose height will make further hops impossible, or it will share the position of more than one neighboring minimum. In the latter case, the calculation of the mass center for the ground state will be necessary to identify the muon position. Inspection of V_μ in three-dimensional systems to understand muon delocalization can be difficult. We need, therefore, a criterion to define the extension of the wave function about a minimum. We use the turning point concept to define the wave-function spreading volume, which we call *localization volume*, which satisfies the condition $V_\mu(\mathbf{r}) < E_0$, where E_0 is the zero-point motion energy [in short, the zero-point energy (ZPE)]. As a rough approximation, in a recent work[37] we computed E_0 by modeling each minimum as an anisotropic harmonic well,

$$V(\mathbf{r}) = \tfrac{1}{2}m_\mu\left(\omega_x^2 x^2 + \omega_y^2 y^2 + \omega_z^2 z^2\right) + V_0, \quad (2)$$

with eigenvalues given by

$$E(n_x,n_y,n_z) = \hbar[\omega_x(n_x+1/2) + \omega_y(n_y+1/2) + \omega_z(n_z+1/2)] + V_0,$$

and a ZPE

$$E_0 = \hbar(\omega_x+\omega_y+\omega_z)/2 + V_0. \quad (3)$$

The anisotropic harmonic well model cannot be used when the potential well surrounding the minimum has an irregular shape, such as in LiF and YF_3. Therefore, here E_0 is given by the eigenvalue of the ground state obtained when solving the Schrödinger equation for the μ^+ particle:

$$\left[\frac{\hbar^2\nabla^2}{2m_\mu} + V_\mu(\mathbf{r})\right]\psi_{\mu,i}(\mathbf{r}) = E_{\mu,i}\psi_{\mu,i}(\mathbf{r}). \quad (4)$$

This procedure allows us to define a corresponding disconnected localization volume for each stopping site. It may also happen that a localization volume goes across the primitive cell boundary and connects neighboring cells. This would imply muon diffusion across the crystal, a possibility that, as we will show, is prevented by the formation of the F-μ^+-F complex.

If the muon did not modify its environment, that procedure would be sufficiently accurate. Instead, muons induce a relaxation of the local neighboring lattice structure. To compute the local lattice relaxation, we neglect the spread of the muon wave function due to the ZPM, and within the DFT framework, we study the effect of muon trapping on the surrounding structure as if it was the trapping process for an interstitial proton. Indeed when the ZPM is neglected, protons and muons are equivalent. Within the pseudopotential formalism, the proton or muon is represented by the hydrogen pseudopotential in the PAW formalism[32] available in the QE database. Since we do not want to reproduce the muon implantation process' actual dynamics, we use a heuristic approach to find the stopping site. We place the charged impurity (i.e., the proton or muon) in the sites identified as minima by the electrostatic potential landscape technique or by insights from experiments. Then we let the system evolve to the ground state allowing both electron rearrangement and lattice distortion. The final optimized position for the impurity represents the refined muon position.

We compute the relaxed lattice structure using a supercell built up from our bulk structure by doubling the bulk primitive cell along each crystal axis direction ($2 \times 2 \times 2$ supercell). A convergence threshold of 5 meV is set for the total energy convergence for structural minimization. Here we want to study the localization of a μ^+, therefore we make use of charged supercells. Since charged supercells cannot be treated with periodic boundary conditions, we use a neutralizing compensating background approach. The accuracy of supercell calculations is limited by the size of the simulation. For neutral light impurities $2 \times 2 \times 2$ supercells may be enough. Since we deal with charged impurities (muon interstitial) we made a convergence test using the SIESTA code.[38] Comparing the structure and total energy of $2 \times 2 \times 2$ and $3 \times 3 \times 3$ supercells, we estimate the numerical error on the energy and on the optimized distances to be $\sim$5 meV and $\sim$0.02 Å, respectively.

III. SOLUTION OF THE SPIN HAMILTONIAN

LiF and YF_3 are especially useful as test cases for our DFT calculations because a precise verification of the muon site is obtained by best fitting the asymmetry signal produced by

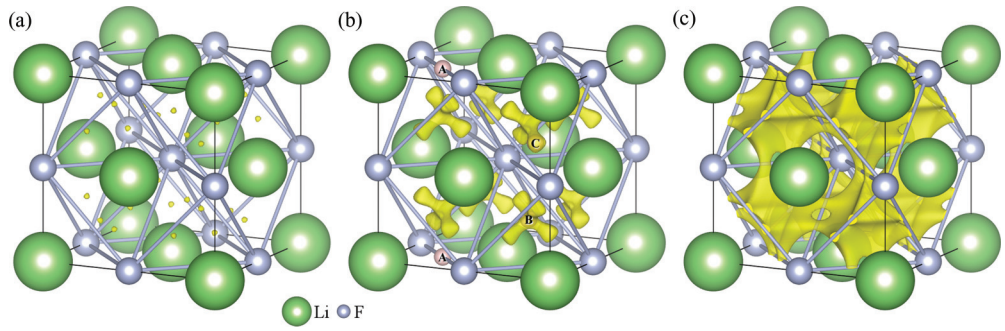

FIG. 1. (Color online) Isosurfaces of the electrostatic potential in LiF for $V_\mu(r) = 50$, 100, and 500 meV in (a), (b), and (c), respectively. The isosurface in (c) represents the *localization volume* (see text) for the muon in the bulk electrostatic potential.

the dipolar interaction between the muon and its neighboring nuclear moments. In fluorides, because of F's high nuclear moment (^{19}F has spin $I = \frac{1}{2}$ and ∼100% natural abundance) and its high electronegativity, the interaction, commonly referred to as F-μ^+-F, is more pronounced. An entangled quantum state develops between the muon and the surrounding nuclei, and the system may be described with the following Hamiltonian:

$$\mathcal{H} = \sum_{i>j} \frac{\mu_0 \gamma_i \gamma_j}{4\pi r^3} [\mathbf{S}_i \cdot \mathbf{S}_j - 3(\mathbf{S}_i \cdot \hat{\mathbf{r}})(\mathbf{S}_j \cdot \hat{\mathbf{r}})], \tag{5}$$

where $\mathbf{r}$ is the vector between spins S_i and S_j of either the fluorine nuclei or the muon, which have gyromagnetic ratios γ_i and γ_j. The muon depolarization is given by

$$G_\zeta(t) = \frac{1}{N} \sum_{m,n} e^{i(\omega_m - \omega_n)t} |\langle m|\sigma_\zeta|n\rangle|^2, \tag{6}$$

where N is the Hilbert space dimension, $|m\rangle$ and $|n\rangle$ are eigenstates of $\mathcal{H}$, $\hbar\omega_{m,n}$ are the corresponding eigenvalues, σ_ζ is the Pauli spin matrix corresponding to the quantization direction, and h is the Planck constant. In a powdered sample with cubic symmetry, the observed signal is given by the weighted average over all directions, i.e.,

$$\overline{|\langle m|\sigma_\zeta|n\rangle|^2} = \frac{1}{3}(|\langle m|\sigma_z|n\rangle|^2 + |\langle m|\sigma_y|n\rangle|^2 + |\langle m|\sigma_x|n\rangle|^2). \tag{7}$$

Since the dipolar interaction is inversely proportional to the cube of the internuclear distance, one usually considers only up to the next-neighboring atoms in order to make the muon polarization calculation computationally inexpensive with a negligible loss of accuracy. Moreover, the coupling between F nuclear spins may often be ignored with a limited loss of accuracy.

For an axially symmetric F-μ^+-F complex, as in the case of LiF, when considering only the two nearest-neighboring F atoms at a distance r from the muon, the analytic solution of Eq. (5) for a powder averaged depolarization is

$$G_p(t) = \frac{1}{6}\left[3 + \cos\sqrt{3}\omega_d t + \left(1 - \frac{1}{\sqrt{3}}\right)\cos\frac{3-\sqrt{3}}{2}\omega_d t + \left(1 + \frac{1}{\sqrt{3}}\right)\cos\frac{3+\sqrt{3}}{2}\omega_d t\right], \tag{8}$$

where $\omega_d = \mu_0 \gamma_F \gamma_\mu h/(2r^3)$. This result allows us to identify the muon site in LiF with the sole use of experimental data; instead, as shown hereafter, Eq. (8) fails to capture the data trend in YF_3, and the F-μ^+-F effect alone is not sufficient to determine the μ^+ site.

IV. LiF

LiF has the NaCl crystal structure, with a four formula unit conventional cubic cell, containing eight cubic cages with vertexes at four Li and four F atoms. As shown in Fig. 1, the minima of the electrostatic potential in LiF are located near the center of each cage. The minima inside the cage are five. The one we label B in Fig. 1(b) is at the very center of the cage surrounded by four equivalent minima labeled C placed in the direction of the neighboring F atoms. The minima become connected for $E \geqslant 75$ meV forming a sort of tetrahedron-shaped structure with a centroid in site B. All these positions are incompatible with the experimental muon sites known from the literature and obtained with the strategy explained in Sec. III.[11] Figure 1(c) shows the μ^+ localization volume according to the ZPE obtained by the solution of the Schrödinger equation for the μ^+ in the bulk electrostatic potential for LiF. We see that the μ^+ is quite delocalized because its localization volume forms a connected network across the crystal. The experimental position, labeled A in Fig. 1(b), is at the boundary of the localization volume.

Muon delocalization inside a strongly polar solid is the condition under which we expect to have a strong effect of μ^+-sample interaction on the outcome of our calculations. Indeed, allowing atom relaxation in the minimum energy configuration we obtain some large atomic displacement from periodic bulk positions for all sites considered here. A strong modification of the crystal structure is found when the muon is added to the interstitial site A. While F nuclei are attracted by the charged impurity, Li atoms are repelled. The distance between the muon and its neighboring F nuclei is 1.15 Å, in excellent agreement with the experimental data. Also next-neighboring F atoms are affected by the μ^+ and are subject to a displacement of 0.04 Å. The relaxed atomic positions correctly describe the formation of a F-μ^+ bonding. The relaxed structure for the muon sitting in site B shows a similar behavior: the distance between the muon and its neighboring F atoms reduces from 1.76 to 1.57 Å. In any case, we note that the F-μ^+ distance in this case is too large to

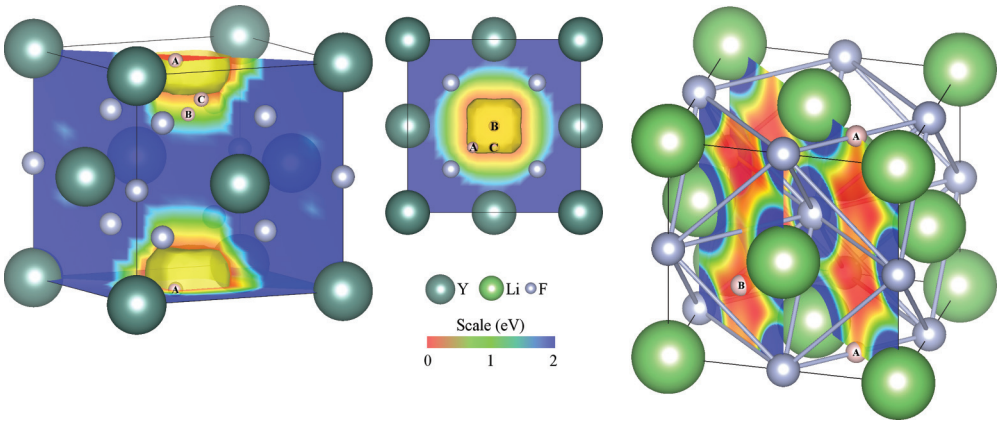

FIG. 2. (Color online) Possible muon sites in YF_3 (left and center) and LiF (right). Label A identifies the expected site in both compounds. *Localization volume* surfaces are shown in dark yellow for YF_3 and in Fig. 1(c) for LiF. Please note that we are showing unrelaxed lattice structures.

reproduce the experimental fast decay of the μSR signal. Site C is a local minimum for the structural relaxation, and this is where a proton would remain trapped. The effect of ZPM here is important, and because of the large delocalization, the muon gets out of the local minimum and reaches site A as a consequence of the gradual atomic position relaxation. This behavior is moreover energetically favored if we look at the total energies for the μ^+-sample system given by our DFT simulations. The total energies for sites A, B, and C are reported in Table I. We see that the inclusion of relaxation effects allows us to recover the agreement with the experimental findings: site A has a total energy which is 0.89 eV lower with respect to site B and is thus confirmed to be the muon stopping site in LiF. The formation of the F-μ^+-F complex has important consequences on μ^+ delocalization in LiF. Indeed, lattice relaxation breaks the lattice periodicity, while the μ^+ forms a bond with F enhancing localization and hindering μ^+ diffusion across the material, in agreement with the experimental evidence.

The results of our calculations are confirmed by a comparison with experimental data. The expected depolarizations for sites A, B, and C are shown in Fig. 3. It is clear that the time dependencies of the muon polarization for the three inequivalent sites are very different, allowing us to discard sites B and C. Only site A is compatible with the observed asymmetry spectra. The other two locations for μ^+ give significantly worse fits (site C) and nonphysical values for the local modification of the bond length and distances between μ^+ and F nuclei (site B). Fitting the experimental results with $\mathbf{r}_{\mu^+-\mathbf{F}}$ as a free parameter in Eq. (5), we find that the distorted crystal structure obtained from DFT calculations reproduces the experimental F-F distance[11] with $\sim$1% precision.

TABLE I. Results for the structural optimization with μ^+ in the interstitial positions A, B, and C (see text and Fig. 2). Site A is always the experimental or predicted site. F-μ^+ is the distance between the μ^+ and its nearest-neighbor F atom(s), $E_i - E_A$ are the DFT ground-state energies of the relaxed structures referred to E_A.

	LiF			YF_3		
	A	B	C	A	B	C
F-μ^+ distance (Å)	1.15	1.56	1.01	0.144	1.134	1.144
$E_i - E_A$ (eV)	0	0.89	0.54	0	−0.64	0.36

V. YF_3

To find the muon sites' positions, DFT calculations are more important in YF_3 than in LiF. First of all, experimental data alone do not allow an unambiguous site identification by the F-μ^+-F signal because too many inequivalent μ^+ interstitial positions are available in the primitive cell. Secondly, the Coulomb potential for the unperturbed bulk crystal shows only one minimum in $(\frac{1}{2},\frac{1}{2},0)$ that yields a depolarization which cannot capture the experimental asymmetry spectra. Moreover, here the depolarization signal is only roughly captured by the *axial* F-μ^+-F expectations as shown in Fig. 4. Therefore, a reliable muon site assignment in YF_3 can only be achieved through DFT calculations. Following the same procedure used with LiF, we relaxed the lattice structure with

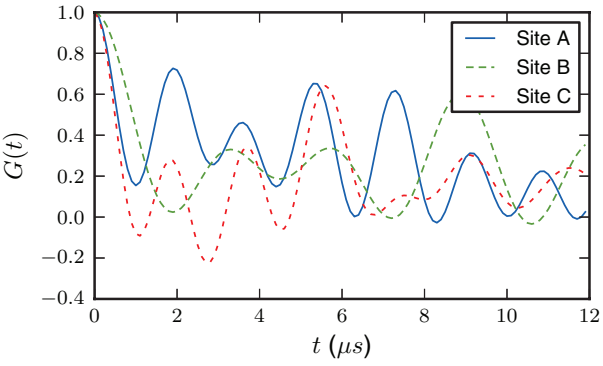

FIG. 3. (Color online) Expected μ^+ asymmetry spectra for optimized muon sites and atomic coordinates in powdered LiF. Sites are labeled as in Fig. 1. Calculations include only the neighboring atoms that give rise to couplings higher than one-tenth of the maximum coupling constant [see Eq. (5); the number of F atoms considered depends on the μ^+ interstitial site]). Position A gives the best agreement with the measured data.[11]

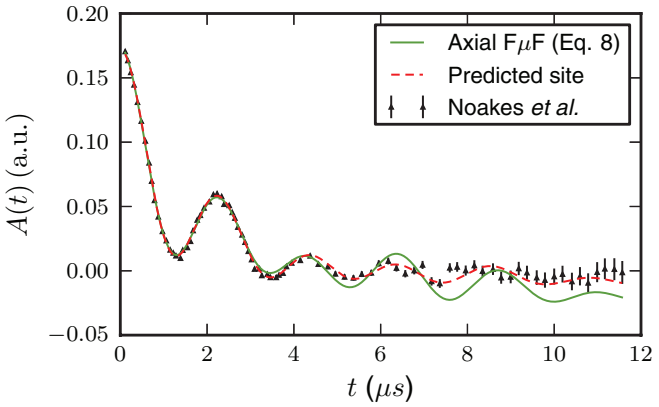

FIG. 4. (Color online) Fit of YF_3 data from Ref. 39 using the conventional F-μ^+-F model [Eq. (8)] and the depolarization calculated for the fully relaxed structure site as predicted by the DFT. The parameters of the fit are detailed in the text and reported in Table III.

muons placed in nonsymmetric interstitial positions. Starting with random interstitial positions, we found six possible inequivalent interstitial sites. The inequivalent sites shown in Fig. 2 are the three most energetically favorable and are all close to the localization volume. They are all characterized by a slightly distorted F-μ^+-F bond where the muon is shifted perpendicular to the F-F axis forming an angle between the two bonds of $\sim$144° for sites A and C and of $\sim$160° for site B (in Fig. 2 the unrelaxed structures are shown for the sake of clarity). The distances between the muon and its first neighboring F nuclei are 1.145 Å for sites A and C and 1.13 Å for site B. The other three sites will not be considered in the rest of this paper for the following reasons: they are too far from the Coulomb potential minimum, they have higher ground-state energies, and they result in depolarization functions which are clearly incompatible with the experimental results.

The depolarizations arising from the relaxed structures of sites A, B, and C are compared in Fig. 5. The relaxed energies

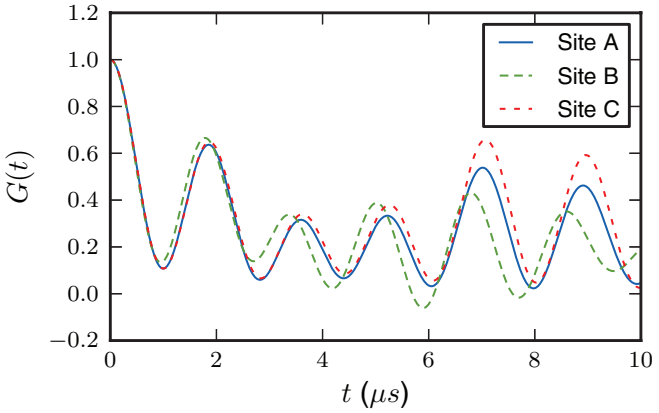

FIG. 5. (Color online) Expected asymmetry spectra for powdered YF_3 using optimized muon sites and atomic coordinates. Sites are labeled as in Fig. 2. Calculations include only the neighboring atoms that give rise to couplings greater than one-tenth of the maximum coupling constant [see Eq. (5)]. Position A gives the best agreement with the measured data.

TABLE II. The zero-point energies (E_0) for the muon in the Coulomb potential minimum and the energies ($E_{A,B,C}$) for the relaxed muon sites in the bulk Coulomb potential. All energies are in eV and only the significant figures are reported.

	E_0	E_A	E_B	E_C
LiF	0.50	0.50	0.07	0.00
YF_3	0.145	0.10	1.08	0.22

with the relevant parameters obtained from the DFT structural relaxation are reported in Table I, while ZPEs and energies for the final muon's positions in the bulk Coulomb potential are given in Table II.

All the above results must be considered in order to identify the muon sites. Indeed, site B does not provide a correct description of the depolarization function (Fig. 6) even if it has the lowest energy in the relaxed structure. On the contrary, as shown in Fig. 4, the expected depolarization from site A provides a good description of the experimental data. Moreover, we point out that kinetics should favor trapping in site A, being the site with the lowest electrostatic potential in the unperturbed bulk structure and the only one inside the μ^+ localization volume of the V_μ global minimum. Both sites B and C have energies higher than the muons' ZPE. Thus the muon is more likely to be found in site A than in sites B and C, and so the formation of a F-μ^+-F complex occurs in A. Based on the results, we conclude that the F-μ^+-F complex in site A is the maximally populated muon site in YF_3. As with LiF, the localization region shrinks as a consequence of the formation of the bond, allowing us to neglect the ZPM when solving Eq. (5)

The experimental data were fitted according to the equation

$$A(t) = A_0\{p_1 G_{F\mu F}(t,\delta\omega)\exp[-(\lambda_{F\mu F}t)^\beta] + p_2\exp[-(\sigma t)^2]\} + A_{\text{calbg}}, \quad (9)$$

where A_0 is the total asymmetry arising from the sample and the sample holder, p_1 measures the fraction of muons reaching the F-μ^+-F site, $p_2 = 1 - p_1$ and σ account for the depolarization in the presence of weak nuclear coupling, and A_{calbg} is added in order to compensate for the background and for the uncertain calibration of the nonprecessing component. $G_{\text{F-}\mu\text{-F}}$ is obtained by solving Eq. (5) with the lattice structure

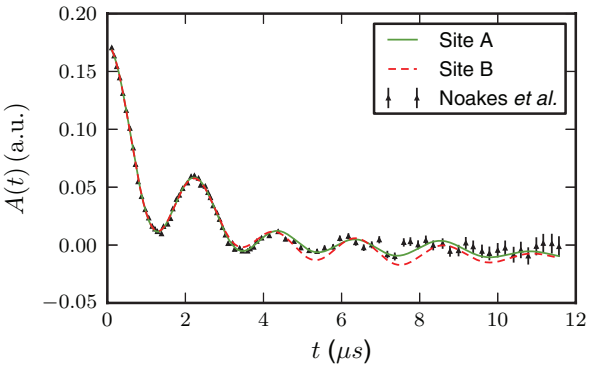

FIG. 6. (Color online) Fit of YF_3 data from Ref. 39 using the depolarization calculated with Eq. (5) for the refined positions obtained from DFT results with regard to sites A and B.

TABLE III. Parameters for Eq. (9) obtained through the best-fit from the data in Fig. 4. In the first column we report the results obtained with $G_{\text{F-}\mu\text{-F}}$ defined in Eq. (8) (already obtained by the authors of Ref. 39). In the second and third columns, $G_{\text{F-}\mu\text{-F}}$ is calculated from DFT results (see text). $r_{\text{F-}\mu}$ is the distance between the muon and the first-neighboring F atom(s) for a given μ^+ site. Small discrepancies between the experimental and calculated $r_{\text{F-}\mu}$ might arise from the reduced but nonvanishing ZPM neglected in Eq. (5). They are accounted for by the $\delta\omega$ parameter (see text). The final F-μ distance is obtained by scaling all the distances between the μ^+ and the atoms included in the sum of Eq. (5). All the scaling factors are smaller than 5%.

	Conv. F-μ^+-F	Site *A*	Site *B*
A_0	0.202(1)	0.184(1)	0.188(1)
p_1	0.77(1)	0.76(1)	0.75(1)
A_{calbg}	−0.028(1)	−0.012(1)	−0.014(1)
$\lambda_{\text{F-}\mu\text{-F}}$	0.18(1) μs^{-1}	0.19(1)	0.15(1)
β	1.27(6)	1.45(1)	1.23(1)
$r_{\text{F-}\mu}$	1.23(1) Å	1.17(1) Å	1.22(1) Å
σ	0.73(1) μs^{-1}	0.97(1) μs^{-1}	1.00(2) μs^{-1}
χ^2_r	4.7	2.3	4.1

obtained from DFT calculations and $\delta\omega$ is a parameter that accounts for small discrepancies between F-μ^+ calculated and experimental distances.

The parameters obtained from the best fits shown in Figs. 4 and 6 are reported in Table III. We point out that, unlike the other sites, for site *A*, which has the lowest chi-square, a smaller correction to the calculated F-μ^+ distances was necessary. We finally highlight that also site *C* is compatible with the experimental data and therefore we cannot rule out the possibility of its partial occupation.

VI. CONCLUSIONS

In this work we show that, in materials in which a strong μ^+-system interaction is present, the correct interpretation of μSR experiments requires a combination of experimental and theoretical investigation. The latter is best done by an *ab initio* approach within DFT. Indeed, DFT is able to provide the electrostatic potential we use to find candidate sites for μ^+ localization and also allows us to get the refined atomic structure we use to understand the experimental data. We tested our procedure in LiF, where we showed that the bulk electrostatic potential fails to correctly predict the actual μ^+ site, while upon structural refinement we were able to reproduce the formation of the F-μ^+-F complex and its structural details (F-μ^+ distance). We then included in our investigation YF_3 where the presence of too many candidate interstitial sites makes the identification of the μ^+ position impossible using only experimental knowledge. In YF_3, we were able to predict the correct location and shape for the F-μ^+-F complex by comparing the experimental data with the refined structure obtained through DFT investigation. We stress that our approach, tested on materials in which μ^+-system interaction is quite large, is of general validity and can be applied to a wide choice of different materials other than just wide band gap insulators.[40,41]

Note added. While completing this work, we became aware of an independent work by Möller and co-workers,[42] who studied muon interactions in fluorides by means of DFT-based *ab initio* calculations. Moeller's results for LiF are consistent with our outcomes. In our work, we extended our investigation to the extremely challenging problem of identifying muon sites in YF_3. Our successful interpretation of the experimental data strongly supports the reliability of our approach.

ACKNOWLEDGMENTS

P.B. and R.D.R. want to acknowledge S. R. Kreitzman, J. Moeller, D. Ceresoli, and T. Lancaster for fruitful discussions. F.B. acknowledges support from CASPUR under the Standard HPC Grant 2012 and from the FP7 European project SUPER-IRON (grant agreement No. 283204). R.D.R. acknowledges support from the European Commission under the 7th Framework Programme through the Key Action: Strengthening the European Research Area, Research Infrastructures, Contract No. CP-CSA_INFRA-2008-1.1.1, No. 226507-NMI3R.

[1] A. Yaouanc and P. de Réotier, Muon Spin Rotation, Relaxation, and Resonance: Applications to Condensed Matter, International Series of Monographs on Physics (Oxford University Press, Oxford, 2010).

[2] S. F. J. Cox, Rep. Prog. Phys. **72**, 116501 (2009).

[3] D. C. Walker, Muon and Muonium Chemistry (Cambridge University Press, Cambridge, 1983).

[4] H. V. Alberto, R. C. Vilão, J. P. Duarte, J. M. Gil, A. Weidinger, J. S. Lord, and S. F. J. Cox, Phys. Rev. B **86**, 035203 (2012).

[5] I. McKenzie, H. Dilger, E. Roduner, R. Scheuermann, and U. Zimmermann, J. Phys. Chem. B **112**, 3070 (2008).

[6] A. Stoykov, R. Scheuermann, K. Sedlak, J. Rodriguez, U. Greuter, and A. Amato, Phys. Procedia **30**, 7 (2012).

[7] S. Cox, J. Phys. C **20**, 3187 (1987).

[8] R. H. Heffner and K. Nagamine, J. Phys.: Condens. Matter **16**, (2004).

[9] E. Roduner, in *Radiation Chemistry Present Status and Future Trends*, Studies in Physical and Theoretical Chemistry Vol. 87, edited by C. D. Jonah and B. M. Rao (Elsevier, Amsterdam, 2001), pp. 83–106.

[10] O. Hartmann, Hyperfine Interact. **49**, 61 (1989).

[11] J. H. Brewer, S. R. Kreitzman, D. R. Noakes, E. J. Ansaldo, D. R. Harshman, and R. Keitel, Phys. Rev. B **33**, 7813 (1986).

[12] J. H. Brewer, K. M. Crowe, F. N. Gygax, R. F. Johnson, B. D. Patterson, D. G. Fleming, and A. Schenck, Phys. Rev. Lett. **31**, 143 (1973).

[13] T. Lancaster, S. J. Blundell, P. J. Baker, M. L. Brooks, W. Hayes, F. L. Pratt, J. L. Manson, M. M. Conner, and J. A. Schlueter, Phys. Rev. Lett. **99**, 267601 (2007).

[14]C. G. Van de Walle, Phys. Rev. Lett. **64**, 669 (1990).
[15]M. Camani, F. N. Gygax, W. Rüegg, A. Schenck, and H. Schilling, Phys. Rev. Lett. **39**, 836 (1977).
[16]R. De Renzi, G. Guidi, P. Podini, R. Tedeschi, C. Bucci, and S. F. J. Cox, Phys. Rev. B **30**, 186 (1984).
[17]K. H. Chow, R. L. Lichti, R. F. Kiefl, S. Dunsiger, T. L. Estle, B. Hitti, R. Kadono, W. A. MacFarlane, J. W. Schneider, D. Schumann, and M. Shelley, Phys. Rev. B **50**, 8918 (1994).
[18]J. Brewer, R. Kiefl, J. Carolan, P. Dosanjh, W. Hardy, S. Kreitzman, Q. Li, T. Riseman, P. Schleger, H. Zhou *et al*. Hyperfine Interact. **63**, 177 (1991).
[19]R. F. Kiefl, M. Celio, T. L. Estle, S. R. Kreitzman, G. M. Luke, T. M. Riseman, and E. J. Ansaldo, Phys. Rev. Lett. **60**, 224 (1988).
[20]T. Estle, S. Estreicher, and D. Marynick, Phys. Rev. Lett. **58**, 1547 (1987).
[21]C. P. Herrero and R. Ramírez, Phys. Rev. Lett. **99**, 205504 (2007).
[22]R. Valladares, A. Fisher, and W. Hayes, Chem. Phys. Lett. **242**, 1 (1995).
[23]D. Cammarere, R. Scheicher, N. Sahoo, T. Das, and K. Nagamine, Physica B **289-290**, 636 (2000).
[24]E. L. Silva, A. G. Marinopoulos, R. C. Vilão, R. B. L. Vieira, H. V. Alberto, J. Piroto Duarte, and J. M. Gil, Phys. Rev. B **85**, 165211 (2012).
[25]R. Scheicher, D. Cammarere, N. Sahoo, T. Briere, F. Pratt, K. Nagamine, and T. Das, Physica B **326**, 30 (2003).
[26]M. Manninen and P. F. Meier, Phys. Rev. B **26**, 6690 (1982).
[27]A. R. Porter, M. D. Towler, and R. J. Needs, Phys. Rev. B **60**, 13534 (1999).
[28]H. Maeter, H. Luetkens, Y. G. Pashkevich, A. Kwadrin, R. Khasanov, A. Amato, A. A. Gusev, K. V. Lamonova, D. A. Chervinskii, R. Klingeler, C. Hess, G. Behr, B. Buchner, and H. H. Klauss, Phys. Rev. B **80**, 094524 (2009).
[29]A. Kerridge, A. H. Harker, and A. M. Stoneham, J. Phys.: Condens. Matter **16**, 8743 (2004).
[30]J. P. Perdew and Y. Wang, Phys. Rev. B **45**, 13244 (1992).
[31]P. Giannozzi, S. Baroni, N. Bonini, M. Calandra, R. Car, C. Cavazzoni, D. Ceresoli, G. L. Chiarotti, M. Cococcioni, I. Dabo, A. Dal Corso, S. de Gironcoli, S. Fabris, G. Fratesi, R. Gebauer, U. Gerstmann, C. Gougoussis, A. Kokalj, M. Lazzeri, L. Martin-Samos, N. Marzari, F. Mauri, R. Mazzarello, S. Paolini, A. Pasquarello, L. Paulatto, C. Sbraccia, S. Scandolo, G. Sclauzero, A. P. Seitsonen, A. Smogunov, P. Umari, and R. M. Wentzcovitch, J. Phys.: Condens. Matter **21**, 395502 (2009).
[32]P. E. Blöchl, Phys. Rev. B **50**, 17953 (1994).
[33]D. Singh, Phys. Rev. B **43**, 6388 (1991).
[34]E. Sjöstedt, L. Nordström, and D. J. Singh, Solid State Commun. **114**, 15 (2000).
[35]P. Blaha, K. Schwarz, G. Madsen, D. Kvasnicka, and J. Luitz, WIEN2K, *An Augmented Plane Wave + Local Orbitals Program for Calculating Crystal Properties* (Karlheinz Schwarz, Techn. Universität Wien, Austria, 2001), http://www.wien2k.at.
[36]M. Bendele, A. Ichsanow, Y. Pashkevich, L. Keller, T. Strässle, A. Gusev, E. Pomjakushina, K. Conder, R. Khasanov, and H. Keller, Phys. Rev. B **85**, 064517 (2012).
[37]R. De Renzi, P. Bonfà, M. Mazzani, S. Sanna, G. Prando, P. Carretta, R. Khasanov, A. Amato, H. Luetkens, M. Bendele, F. Bernardini, S. Massidda, A. Palenzona, M. Tropeano, and M. Vignolo, Supercond. Sci. Technol. **25**, 084009 (2012).
[38]J. M. Soler, E. Artacho, J. D. Gale, A. García, J. Junquera, P. Ordejón, and D. Sanchez-Portal, J. Phys.: Condens. Matter **14**, 2745 (2002).
[39]D. R. Noakes, E. J. Ansaldo, S. R. Kreitzman, and G. M. Luke, J. Phys. Chem. Solids **54**, 785 (1993).
[40]G. Prando, P. Bonfà, G. Profeta, R. Khasanov, F. Bernardini, M. Mazzani, E. M. Brüning, A. Pal, V. P. S. Awana, H.-J. Grafe, B. Büchner, R. De Renzi, P. Carretta, and S. Sanna, Phys. Rev. B **87**, 064401 (2013).
[41]G. Lamura, T. Shiroka, P. Bonfà, S. Sanna, F. Bernardini, R. De Renzi, R. Viennois, E. Giannini, A. Piriou, N. Emery, M. R. Cimberle, and M. Putti, J. Phys.: Condens. Matter **25**, 156004 (2013).
[42]J. S. Möller, D. Ceresoli, T. Lancaster, N. Marzari, and S. J. Blundell, Phys. Rev. B **87**, 121108(R) (2013).